IMPACT OF LIGAND STRUCTURES ON PRECIPITATION KINETICS OF URANYL NITRATE COORDINATION POLYMERS WITH DIAMIDE LINKERS

Makito Nojima[1], Satoru Tsushima[1,2], and Koichiro Takao[1*]

[1]Laboratory for Zero-Carbon Energy, Institute of Integrated Research, Institute of Science Tokyo, N1-32, 2-12-1, O-okayama, Meguro-ku, Tokyo 152-8550 Japan.
[2]Institute of Resource Ecology, Helmholtz-Zentrum Dresden-Rossendorf, Bautzner Landstraβe 400, 01328 Dresden, Germany.
* Corresponding author

Abstract. The structure of uranyl nitrate complexes with four different diamide ligands with *trans*-1,4-cyclohexyl bridging moieties (two cyclic diamides (**L1**: γ-lactam, **L2**: δ-lactam) and two acyclic diamides with different linear chains (**L3**: Me, **L4**: Et)) and the effect of different ligand structures on the rate of precipitation formation were examined. **L2**, **L3**, and **L4** formed 1D coordination polymers $[UO_2(NO_3)_2(\mathbf{Lx})]_n$ (x = 2-4) in a similar manner to the previously reported case of **L1**. In use of the cyclic diamides, **L1** and **L2**, the precipitation formation started right after loading these precipitants, and rapidly proceeded. On the other hand, use of the acyclic diamides, **L3** and **L4**, exhibited induction period for more than the first 60 minutes prior to the precipitation formation, and even after that, slower precipitation rate was observed.

1. Introduction

Recovery of nuclear materials (U and Pu) from spent nuclear fuels is an important task, and therefore various processes have been developed so far [1]. In the current spent fuel reprocessing, PUREX (Plutonium Uranium Redox EXtraction) is the *de facto* standard. This separation method extracts UO_2^{2+} and Pu^{4+} by tri-*n*-butyl phosphate (TBP) selectively and efficiently. While it guarantees high selectivity, the presence of phosphorus in the ligand makes it difficult to reduce final waste volume even after its incineration. Therefore, several reprocessing principles using amide ligands have been proposed as advanced nuclear fuel reprocessing technologies. The amide ligands usually exhibit strong affinity with UO_2^{2+} and M^{4+} (M = Pu, Th), and well meet requirements from the "CHON" principle and radiation resistivity [2, 3].

There are two main streams of such advanced spent fuel reprocessing methods, *i.e.*, solvent extraction and precipitation. In the former method, *N,N*-dialkylated monoamides [4-6] are usually employed, which prefer to form stable complexes with UO_2^{2+} and M^{4+} to be recycled. As a result, these metal ions significantly tend to be extracted from HNO_3(aq) to an organic phase. In this separation principle, precipitation of any materials must be prevented for the process feasibility. This situation is much different in the other trend, precipitation-based reprocessing, where UO_2^{2+} and M^{4+} will be recovered by their selective and efficient crystallization from the feed solution dissolving the spent fuels. In this reprocessing concept, well-designed amide ligands such as 2-pyrrolidone or γ-lactam derivatives (e.g., **L1**, Fig. 1) may afford sparingly soluble crystalline nitrato complexes of UO_2^{2+} and M^{4+} from HNO_3(aq) [7-9]. In this principle, crystallization with amide ligands must be enhanced for efficient recovery of the nuclear fuel materials.

Hence, knowing what determines formation of precipitates is one of the largest concerns to design and optimize molecular structures of amide ligands to be employed in these advanced reprocessing principles having the conflicting requirements mentioned above. While steric effects of different ligand

structures have been proposed to explain UO_2^{2+}/Pu^{4+} selectivity found in the solvent extraction [10], no details have been well discussed yet on how to control precipitation through the spent fuel reprocessing. Kinetic aspects of precipitates formation are also important, while only a few reports are available to date [11,12].

In this study, we examined the Impact of ligand structures on precipitation kinetics of uranyl nitrate coordination polymers with diamide linkers. The four ligands shown in Fig. 1 were employed for this purpose.

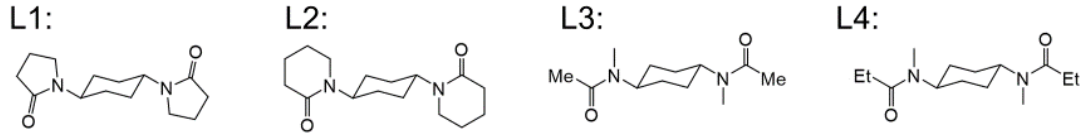

Fig. 1. Schematic structure of diamide ligand employed in this study

2. Experimental

2.1 Materials and Method

Caution! All the isotopes in natural uranium are α emitters, and contain their radioactive daughters. Therefore, standard precautions for handling radioactive materials should be followed. ^{1}H NMR spectra were recorded by using a JEOL ECX-400 (^{1}H: 399.78 MHz) NMR spectrometer. The chemical shifts of ^{1}H NMR were referenced to TMS (δ = 0 ppm). Elemental analyses were carried out by using a Yanaco MT-6 CHN elemental analyzer.

2.2 Synthesis of ligands

While **L1** was prepared as reported elsewhere [9], **L2**-**4** were synthesized as illustrated in Fig. 2.

*2.2.1 Characterization of **L2***

Total yield was 22 %. ^{1}H NMR (δ/ppm vs. TMS, $CDCl_3$, 399.78 MHz): 4.52 (br, 1.99H, N-C_{yc}), 3.71 (t, 4.00 H, 6-CH_2), 2.39 (t, 3.97H, 3-CH_2), 1.82-1.69 (m, 16.61H, 4-CH_2, 5-CH_2, $C_{cy}H_2$). ^{13}C NMR (δ/ppm vs. TMS, $CDCl_3$, 100.53 MHz):169.5, 50.9, 41.8, 32.7, 28.1, 23.4, 21.0.

*2.2.2 Characterization of **L3***

Total yield was 35 %. ^{1}H NMR (δ/ppm vs. TMS, $CDCl_3$, 399.78 MHz): 4.50-4.40 (m, 1.45H, N-$C_{cy}H$), 3.54-3.47 (m, 0.56H, N-$C_{cy}H$), 2.87-2.80 (m, 5.97H, N-CH_3), 2.16-2.05 (m, 6.00H, CO-CH_3), 1.87-1.49 (m, 8.75H, $C_{cy}H_2$). ^{13}C NMR (δ/ppm vs. TMS, $CDCl_3$, 100.53 MHz): 170.5, 170.0, 51.1, 50.7, 30.7, 30.5, 29.6, 28.6, 28.4, 28.3, 22.7, 22.5, 21.8, 21.7, 21.3.

*2.2.3 Characterization of **L4***

Total yield was 35 %. ^{1}H NMR (δ/ppm vs. TMS, $CDCl_3$, 399.78 MHz): 4.52-4.41 (m, 1.43H, N-$C_{cy}H$), 3.60-3.51 (m, 0.53H, N-$C_{cy}H$), 2.85-2.81 (m, 5.93H, N-CH_3), 2.40-2.29 (m, 3.81H, CO-CH_2), 1.84-1.54 (m, 7.99H, $C_{cy}H_2$), 1.18-1.12 (m, 6.00H, CO-C-CH_3). ^{13}C NMR (δ/ppm vs. TMS, $CDCl_3$, 100.53 MHz): 173.6, 173.2, 51.3, 51.0, 29.8, 29.5, 28.7, 28.5, 28.3, 27.7, 27.4, 27.3, 26.8, 9.4, 9.3.

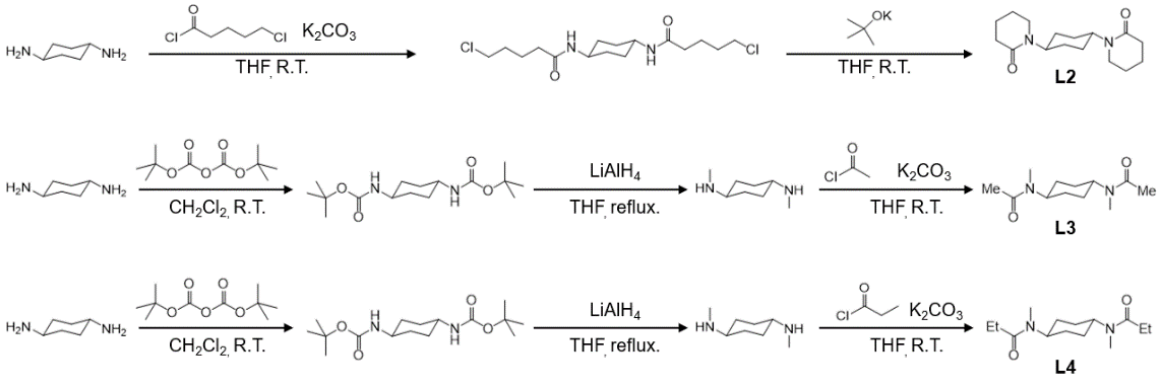

Fig. 2. Synthetic procedure of L2-4 [13, 14].

2.3 Crystallographic Analysis.

The X-ray diffraction data of the well-shaped single crystals of $[UO_2(NO_3)_2(\mathbf{Lx})]_n$ (x = 2-4) were collected by using a Rigaku XtaLAB mini II equipped with a hybrid pixel array detector and using graphite monochromated Mo Kα radiation (λ = 0.71073 Å) at room temperature. Each sample was mounted on a MiTeGen Dual Thickness MicroMounts. Intensity data were collected by taking oscillation photographs. Reflection data were corrected for both Lorentz and polarization effects.

Table 1. Crystal data of $[UO_2(NO_3)_2(\mathbf{Lx})]_n$ (x = 1-4).

ligand	L1	L2	L3	L4
formula	$C_{14}H_{22}N_4O_{10}U$	$C_{16}H_{26}N_4O_{10}U$	$C_{12}H_{22}N_4O_{10}U$	$C_{14}H_{26}N_4O_{10}U$
formula weight	644.38	672.44	620.36	648.42
crystal system	triclinic	monoclinic	monoclinic	monoclinic
space group	*P*-1	$P2_1/n$	$C2/c$	$P2_1/n$
a / Å	5.8962(4)	9.3179(2)	13.1575(7)	10.5752(2)
b / Å	7.6330(6)	9.9653(4)	9.5536(6)	9.2160(2)
c / Å	11.0279(9)	11.7590(3)	15.2173(10)	11.4791(3)
α / °	76.841(5)	90	90	90
β / °	84.480(6)	95.632(2)	95.715(6)	99.422(2)
γ / °	76.229	90	90	90
V / Å^3	468.93(6)	1086.62(6)	1903.3(2)	1103.67(4)
Z	1	2	4	2
T / K	93	293	293	293
D_{calcd} / g·cm^{-3}	2.281	2.055	2.165	1.951
R_1 ($I > 2\sigma$)	0.0174	0.0460	0.0203	0.0392
wR_2 (all)	0.0393	0.0726	0.0493	0.0677
GOF	1.042	1.131	1.073	1.056
CCDC No.	1573161	2386940	2386941	2386942
ref	[9]	this work	this work	this work

The structures were solved by the direct method and refined anisotropically by the SHELX program suite [15, 16] for non-hydrogen atoms by full-matrix least-squares calculations. Each refinement was continued until all shifts were smaller than one-third of the standard deviations of the parameters involved. Hydrogen atoms were refined as riding on their parent atoms with U_{iso}(H) =1.2U_{eq}(C). All calculations were performed by using the Olex2 crystallographic software program package [17]. Crystallographic data of $[UO_2(NO_3)_2(\mathbf{Lx})]_n$ (x = 2-4) were summarized in Table 1, and deposited to Cambridge Crystallographic Data Centre with the accession codes: CCDC 2386940-2386942.

2.4 Precipitation behaviour of $UO_2(NO_3)_2(L)]_n$ in HNO_3

Uranyl nitrate hexahydrate and 60% HNO_3(aq) were together dissolved in distilled water to prepare a stock solution of 0.5 M UO_2^{2+} in 3.0 M HNO_3(aq). **Lx** (x = 1-4) and 60% HNO_3(aq) were together dissolved in distilled water to prepare a stock solution of 0.5 M **Lx** (x = 1-4) in 3.0 M HNO_3(aq). These were appropriately loaded to a separated vial to prepare a sample solution containing 69 mM UO_2^{2+} and 77 mM **Lx** (x = 1-4) in total. It was placed in a thermostatic chamber at 25 ± 1 °C, and the supernatants were periodically collected. Concentrations of UO_2^{2+} remaining in the supernatants (C_{sup}) and that in the stock solution (C_{ini}) were determine by ICP-AES (Thermo Scientific, iCAP7200Duo). The precipitation ratio (*ppt*, -) of UO_2^{2+} were evaluated as follows.

$$ppt = (C_{ini} - C_{sup})/\ C_{ini} \qquad (1)$$

3. Result and discussion

3.1 Molecular and Crystal Structures of $[UO_2(NO_3)_2(Lx)]_n$ (x = 1-4)

In all ligand systems, CHN elemental analyses indicated that the obtained yellow crystals had a common chemical composition, $UO_2(NO_3)_2(\mathbf{Lx})$ (x = 2-4).

Fig. 3 shows the molecular structures of $[UO_2(NO_3)_2(\mathbf{Lx})]_n$ coordination polymers (x = 2, 3, 4) determined by single crystal X-ray diffraction. In all compounds, the central U atom is surrounded by two O_{yl} atoms at the apical positions, four O_{NO3} atoms of the bidentate NO_3^- and two O_L atoms of the monodentate diamide ligands at the trans positions of the equatorial plane of UO_2^{2+}, forming a hexagonal bipyramidal coordination geometry. The $UO_2(NO_3)_2$ units are bridged by diamide ligands, **Lx**. In a similar manner to $[UO_2(NO_3)_2(\mathbf{L1})]_n$ we reported previously [7, 9], formation of one-dimensional coordination polymers of $[UO_2(NO_3)_2(\mathbf{Lx})]_n$ (x = 2, 3, 4), was confirmed here.

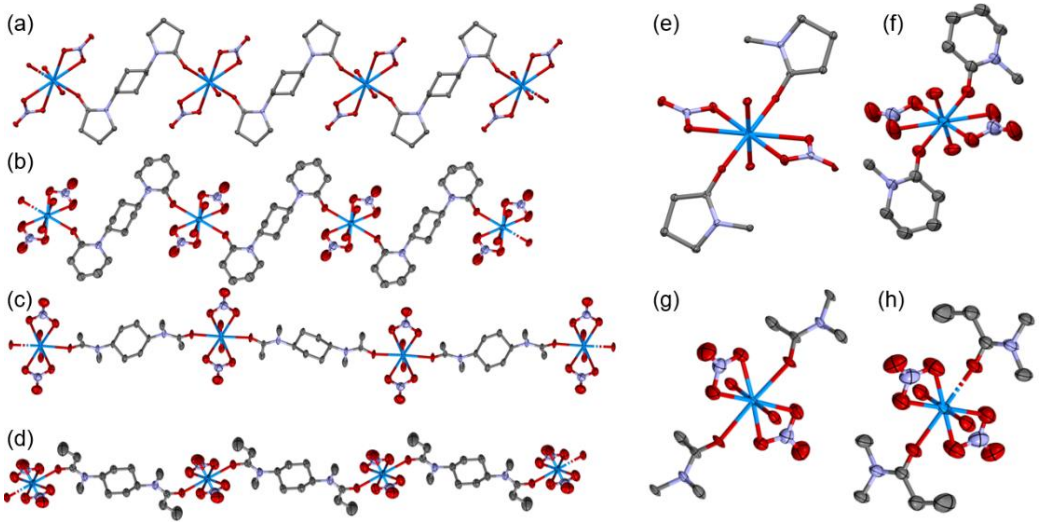

*Fig. 3. Molecular structures of 1D coordination polymers of $[UO_2(NO_3)_2(\mathbf{Lx})]_n$ and their local geometry around U (**Lx** = **L1** (a, e), **L2** (b, f), **L3** (c, g), **L4** (d, h)). Thermal ellipsoids were drawn at 50% probability level. Hydrogen atoms were omitted for clarity. Blue: U, red: O, blue-purple: N, and gray: C.*

Table 2. Selected bond lengths and bond angles of $[UO_2(NO_3)_2(\mathbf{Lx})]_n$ (x = 1-4).

Ligand	L1 [9]	L2	L3	L4
Length / Å				
$U-O_{yl}$	1.769(2)	1.747(4)	1.767(3)	1.751(3)
			1.773(3)	
$U-O_{NO3}$	2.546(2)	2.517(4)	2.511(3)	2.539(3)
	2.550(2)	2.536(4)	2.510(3)	2.342(2)
$U-O_L$	2.362(2)	2.381(3)	2.3695(18)	2.342(2)
O_L-C_L	1.260(4)	1.261(5)	1.264(3)	1.259(4)
C_L-N_L	1.329(4)	1.326(6)	1.318(3)	1.322(5)
Angle / °				
$U-O_L-C_L$	134.4(2)	142.4(3)	141.76(17)	149.9(3)
$O_{yl}-U-O_{yl}$	180	180	180	180

The selected bond lengths and angles in $[UO_2(NO_3)_2(\mathbf{Lx})]_n$ (x = 1-4) were summarized in Table 2. $U-O_{yl}$ is 1.747(4)-1.769(2) Å, which is commonly found in the known uranyl complexes [18]. In the free amide structure, the O_L-C_L distances are usually reported to be 1.23–1.24 Å [19]. On the other hand, those of the O_L-C_L bonds in $[UO_2(NO_3)_2(\mathbf{Lx})]_n$ are 1.259(4)-1.264(3) Å. As reported previously, this trend is due to the delocalization of electrons by coordination [20]. The $O_{yl}-U-O_{yl}$ bond angle was 180° owing to the typical centrosymmetric structure of UO_2^{2+} ($[UO_2(NO_3)_2(\mathbf{Lx})]_n$ (x = 1, 2, 4)) and 2-fold axis ($[UO_2(NO_3)_2(\mathbf{L3})]_n$).

3.2 Precipitation Kinetics of the $[UO_2(NO_3)_2(L)]_n$

The effect of different ligand structures on the rate of precipitates formation was investigated. The obtained results were further analyzed by using the Avrami-Erofe'ev equation, Eq. (2) [21].

$$\alpha = 1 - \exp[-(kt)^n] \qquad (2)$$

where α is the reaction rate, k is the kinetic constant, t is the elapsed time, and n is the Avrami coefficient. This method has been utilized to explain the precipitation kinetics of other uranyl nitrate amide complexes [11, 12]. The observed variation of precipitation ratio for each ligand (**Lx** (x = 1-4)) with elapsed time and the best fit curve based on Eq. (2) are shown in Fig. 4. The best fit parameters obtained by the least-squares regression to Eq. (2) are shown in Table 3.

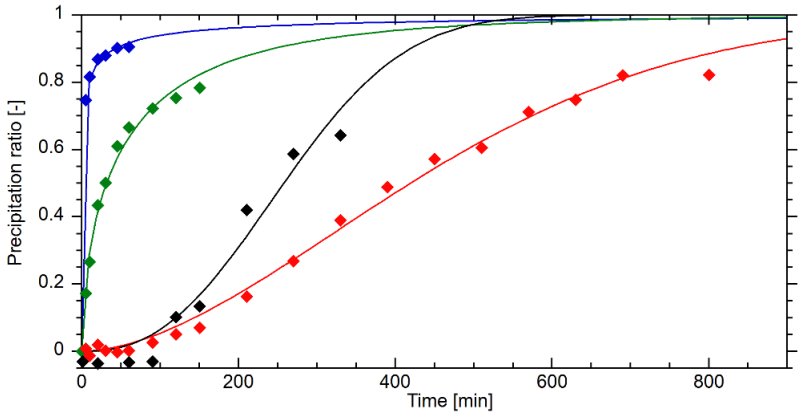

*Fig. 4. Kinetic curves of precipitation ratios of $[UO_2(NO_3)_2(\mathbf{Lx})]_n$ (x = 1-4) from 3 M HNO_3(aq). **L1**: red, **L2**: blue, **L3**: green and **L4**: black.*

When cyclic diamides, **L1** and **L2**, were employed, precipitation of $[UO_2(NO_3)_2(\mathbf{Lx})]_n$ immediately started after mixing the ligands and uranyl nitrate solution. Especially, *k* of **L1** is 0.9(2) min^{-1}, which is the highest in the mono- and diamide ligands for precipitation recovery of UO_2^{2+} developed so far (*e.g.*, *N*,*N*′-bis(*N*″,*N*″-diethyl carbamoyl)piperazine: 0.25(1) min^{-1}, [U] = 20 g L^{-1}, L/U = 1.5 [11]; *N*-(1-adamantyl)acetamide: 0.0214(7) min^{-1}, [U] = 60 g L^{-1}, L/U = 5 [12]).

Table 3. Kinetic parameters extracted from the cure fits from the Avrami-Efofe'ev equation.This fitting was performed Kaleidagraph 5.01. R^2 represent correlation coefficient from the kinetics curves fitting.

Ligand	*n* [-]	*k* [min^{-1}]	R^2 [-]
L1	0.23(2)	0.9(2)	0.976
L2	0.58(4)	0.0170(9)	0.989
L3	1.76(7)	0.00194(3)	0.994
L4	2.4(3)	0.0033(2)	0.939

When acyclic diamides, **L3** and **L4**, were used, precipitation of $[UO_2(NO_3)_2(\mathbf{Lx})]_n$ is much slower than those in use of **L1** and **L2**, and no precipitation has been observed during the initial 1 h. Despite similarity in the precipitation ratios at the final stages of the **L2** and **L3** cases, 8-fold difference in *k* has been found, implying that kinetics of this chemistry is not closely related to its thermodynamics. The slow precipitation rate in use of these acyclic diamides (**L3**, **L4**) would be related to rotational isomerism of them. As illustrated in Fig. 5(a), an O=C-N moiety of the amide group shows the charge-separated resonance arising from electron delocalization of the lone pair on N. As a result, rotation around its C-N bond to switch positions of R_2 and R_3 substituents on N is energetically hindered to afford rotational isomers [22]. Indeed, we have confirmed such an isomerism in **L3** and **L4** by ^{1}H NMR, where three different forms of (*trans, trans*), (*trans, cis*), and (*cis, cis*) shown in Fig. 5(b) are likely to occur in the sample solution.

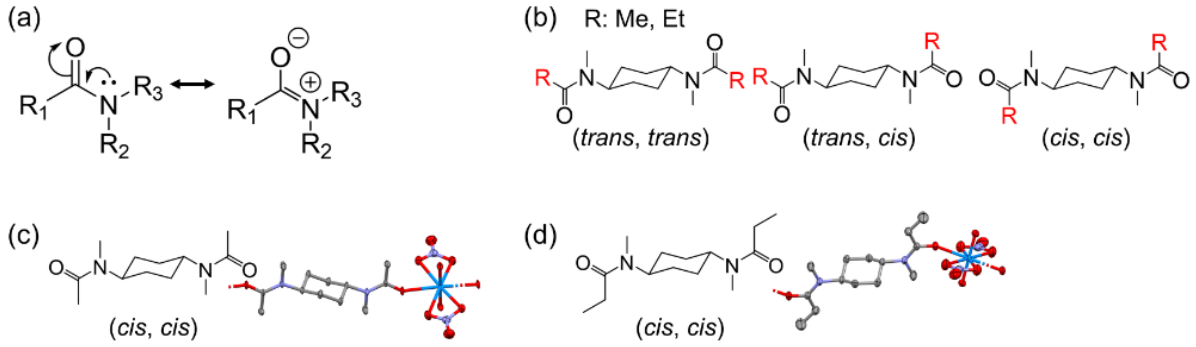

*Fig. 5. Rotational isomerism of acyclic diamides (L3, L4) studied here. (a) Charge-separated resonance form of amide bond. (b) Three possible rotational isomers of the acyclic diamides. (c) **L3** and **L4** conformers found in their $[UO_2(NO_3)_2(\mathbf{Lx})]_n$ crystal structures (see Fig. 5(c) and (d)).*

On the other hand, only (*cis, cis*) isomer occurs in the crystal structures of $[UO_2(NO_3)_2(\mathbf{Lx})]_n$ of **L3** and **L4** (Fig. 5(c) and (d)). Therefore, the rotational barrier around the amide C-N bond must be overcome. Interestingly, this is not the case for **L1** and **L2**, because one of substituents on N is interlocked to the carbonyl C through the lactam ring to prevent the rotation around the amide C-N bond. This is the reason why the faster precipitation kinetics with **L1** and **L2** has been observed in Fig. 4. We have demonstrated that the rate of precipitates formation is able to be controlled by molecular design of the diamide precipitant.

4. Conclusion

In this work, impact of amide ligand structure on the rate of precipitates formation of uranyl nitrate coordination polymers was investigated. Among them, cyclic diamides (**L1**, **L2**) having the different numbers of ring members and acyclic ones (**L3**, **L4**) were examined. **L2**, **L3**, and **L4**, used for the first time in this study commonly provided 1D coordination polymers of $[UO_2(NO_3)_2(\mathbf{Lx})]_n$ (x =2-4) from 3 M HNO_3(aq) in a similar manner to **L1** we reported previously [9]. In contrast, precipitation kinetics significantly depends on the molecular structures of the diamides. The cyclic diamides (**L1**, **L2**) showed higher rates of $[UO_2(NO_3)_2(\mathbf{Lx})]_n$ precipitation, while the acyclic ones (**L3**, **L4**) exhibited slower kinetics of $[UO_2(NO_3)_2(\mathbf{Lx})]_n$ deposition. Such a difference in precipitation kinetics of $[UO_2(NO_3)_2(\mathbf{Lx})]_n$ is ascribed to possibility of the rotational isomerism in the amide groups in the molecular structures of these diamide ligands. Thus, the acyclic diamides must surmount the rotational barrier to become an appropriate structure to form $[UO_2(NO_3)_2(\mathbf{Lx})]_n$, while the cyclic ones already have suitable forms for crystallization of $[UO_2(NO_3)_2(\mathbf{Lx})]_n$.

Acknowledgements

This work was supported by Fostering Joint International Research (B) (JP20KK0119) and Grant-in-Aid for Challenging Research (Pioneering) (JP24K21238) of Japan Society for the Promotion of Science as well as by the WRH Program, IRFI of Institute of Science Tokyo.

References

[1] H.W. Levi, T.H. Pigford, M. Benedict, Nuclear Chemical Engineering (McGraw-Hill College, New York, 1981)
[2] S.A. Ansari, P. Pathak, P.K. Mohapatra, V.K. Manchanda, Chem. Rev. 112, 3 (2012)
[3] G.P. Horne, S.P. Mezyk, B.J. Mincher, C.A. Zarzana, C. Raea, R.D. Tillotson, N.C. Schmitt, R.D. Ball, J. Ceder, M.-C. Charbonnel, P. Guilbaud, G.S. Louis, L. Berthon, Radiat. Phys. Chem. 170, 108608 (2020)
[4] T.H. Siddall III, J. Phys. Chem. 64, 12 (1960)
[5] N. Condamines, C. Musikas, Solvent Extr. Ion Exch. 6, 6 (1988)
[6] N. Tsutsui, Y. Ban, H. Sagawa, S. Ishii, T. Matsumura, Solvent Extr. Ion Exch. 35, 6 (2017)
[7] K. Takao, Y. Ikeda, Eur. J. Inorg. Chem. 36, 3443 (2020)
[8] K. Takao, H. Kazama, Y. Ikeda, S. Tsushima, Angew. Chem. Int. Ed. 58, 1(2019)
[9] H. Kazama, S. Tsushima, Y. Ikeda, K. Takao, Inorg. Chem. 56, 21 (2017)
[10] D.R. Prabhu, G.R. Mahajan, G.M. Nair, J. Radioanal. Nucl. Chem. 224, 113 (1997)
[11] B.G. Vats, A. Bhattacharyya, K. Sanyal, M. Kumar, J.S. Gamare, S. Kannan, Inorg. Chem. 60, 23 (2021)
[12] G. Loubert, N. Henry, C. Volkringer, S. Duval, C. Tamain, B.A-. Chapelet, T. Delahaye, T. Loiseau, Inorg. Chem. 59, 16 (2020)
[13] E.C. Wang, H.-J. Lin, Heterocycles 48, 3 (1998)
[14] S.K. Gediya, V.K. Vyas, G.J. Clarkson, M. Wills, Org. Lett. 23, 20 (2021)
[15] G.M. Sheldrick, Acta Crystallogr. C Struct. Chem. 71, 3 (2015)
[16] G.M. Sheldrick, Acta crystallogr., A 64, 112 (2008)
[17] O.V. Dolomanov, L.J. Bourhis, R.J. Gildea, J.A.K. Howard, H. Puschmann, J. Appl. Crystallogr. 42, 339 (2009)
[18] P.C. Burns, R.C. Ewing, F.C. Hawthorne, Can. Mineral. 35, 6 (1997)
[19] O. Clement, B.M. Rapko, B.P. Hay, Coord Chem Rev 170, 1 (1998)
[20] E. Acher, Y.H. Cherkaski, T. Dumas, C. Tamain, D. Guillaumout, N. Boubals, G. Javierre. C. Hennig, P.L. Solari, M.-C. Charbonnel, Inorg. Chem. 55, 11 (2016)
[21] E.E. Finney, R.G. Finke, Chem. Mater. 21, 19 (2009)
[22] G.N. Radael, R.M. Pontes, Comput Theor Chem 1187, 112938 (2020)